
SHAPE OPTIMIZATION FOR THE MITIGATION OF COASTAL EROSION VIA SMOOTHED PARTICLE HYDRODYNAMICS

 **Luka Schlegel**

Department of Mathematics
Universität Trier
Universitätsring 15, 54296 Trier
schlegel@uni-trier.de

 **Volker Schulz**

Department of Mathematics
Universität Trier
Universitätsring 15, 54296 Trier
volker.schulz@uni-trier.de

March 21, 2022

ABSTRACT

Adjoint-based shape optimization most often relies on Eulerian flow field formulations. However, since Lagrangian particle methods are the natural choice for solving sedimentation problems in oceanography, extensions to the Lagrangian framework are desirable. For the mitigation of coastal erosion, we perform shape optimization for fluid flows, that are described by incompressible Navier-Stokes equations and discretized via Smoothed Particle Hydrodynamics. The obstacle's shape is hereby optimized over an appropriate cost function to minimize the height of water waves along the shoreline based on shape calculus. Theoretical results will be numerically verified exploring different scenarios.

Keywords Shape Optimization · SPH · Coastal Erosion

1 Introduction

Coastal erosion describes the displacement of land caused by destructive sea waves, currents or tides. Major efforts have been made to mitigate these effects using groins, breakwaters and various other structures. Numerical investigations of useful shapes require accurate descriptions of propagating waves and sediment. Lagrangian particle movements appear to be the natural choice for solving sedimentation problems in oceanography, being generally free of diffusion. In contrast, inherent numerical diffusion in Eulerian methods can only affect the resolution of purely advective flows. It is therefore tempting to investigate shape optimization techniques for Lagrangian fluid flows. Typically, meshfree particle methods can be divided in two groups, the ones that approximate the weak form, e.g. the Diffusive Element [1], the Element Free Galerkin [2] or the Reproducing Kernel method [3], or the ones that approximate the strong form, e.g. the Moving Particle [4] or the Vortex method [5]. In this paper we will investigate a particle flow that falls into the latter class - the Smoothed Particle Hydrodynamics (SPH) [6]. Both groups share the property that shape optimization has been only rarely investigated. In general most approaches are based on the weak form, introduced in order to enable large deformations, e.g. for the Element Free Galerkin method [7] or the reproducing kernel particle method [8][9]. Lately a one-way coupled, volume averaged transport model was used to circumvent the direct usage of the Lagrangian particle flow [10]. In particular for SPH fluids only boundary contributions via ghost particles and the direct differentiation method to obtain optimal fluid-structure interaction have been investigated [11]. However, this method comes with the drawback of solving an additional problem for each design parameter, which can become costly for highly resolved obstacles. Hence, adjoint-based shape optimization for SPH fluids and accordingly also the usage in mitigation of coastal erosion appears novel.

The paper is structured as follows: We derive adjoints for a general class of particle systems in Section 2, before Section 3 will build the foundation for modelling a certain particle system described by SPH-fluids, addressing boundary interactions via signed-distance fields [12]. Subsequently, Section 4 will derive shape derivatives based on the adjoints that have been developed for the general case. The technique boils down to derive shape derivatives for a finite element interpolator building up on discrete investigations [13][14]. The results are numerically verified in simplified scenarios using a gradient-descent algorithm. For this, solutions to incompressible Navier-Stokes equations are obtained via

SPH discretization, partial derivatives required for recursive adjoints are calculated via automatic differentiation and a deformation gradient is obtained from linear elasticity evaluations [15].

2 Adjoint for Particle Systems

In this section adjoints for a system of particles consisting of position and velocities $X_k = (x_k, v_k) \in \mathbb{R}^N \times \mathbb{R}^N$ for time steps $k \in \{1, \dots, n\}$ with constant particle mass $m \in \mathbb{R}^+$ are derived. The iteration laws are described by a Symplectic Euler, i.e. for force functions $f : (\mathbb{R}^N \times \mathbb{R}^N \times \Psi) \rightarrow \mathbb{R}^N$ and to be determined control $q \in \Psi$, we solve

$$\begin{aligned} v_k &= v_{k-1} + \frac{\Delta t}{m} f(v_{k-1}, x_{k-1}, q) \\ x_k &= x_{k-1} + \Delta t v_k. \end{aligned} \quad (1)$$

The solution of the particle system constrains a time-dependent objective function $J : (\mathbb{R}^{nN} \times \mathbb{R}^{nN} \times \Psi) \rightarrow \mathbb{R}$, i.e.

$$J(v, x, q) = \sum_{k=1}^n J_k(v_k, x_k, q). \quad (2)$$

In this setting, we can derive the following theorem, consisting of recursively defined adjoints and an equation for the sensitivity calculation with respect to control q .

Theorem 1. *Assume a particle system is solved iteratively using iteration (1), then sequences $\{\delta_k\}_{k=1}^n$ and $\{\mu_k\}_{k=1}^n$ required in adjoint computations are obtained from backward recursion, i.e.*

$$\delta_k = \delta_{k+1} + \frac{\Delta t}{m} (f^{x_k})^T \mu_{k+1} + \frac{\Delta t^2}{m} (f^{x_k})^T \delta_{k+1} + (J_k^{x_k})^T \quad (3)$$

$$\mu_k = \mu_{k+1} + \frac{\Delta t}{m} (f^{v_k})^T \mu_{k+1} + \frac{\Delta t}{m} \delta_{k+1} + \frac{\Delta t^2}{m} (f^{v_k})^T \delta_{k+1} + (J_k^{v_k})^T, \quad (4)$$

where the recursion starts at

$$\mu_n = J_n^{v_n} \quad \delta_n = J_n^{x_n} \quad (5)$$

and the superscript denotes the respective partial derivative. The sensitivity of the objective function with regards to the control q are calculated as

$$J^q = \sum_{k=1}^n J_k^q + \frac{\Delta t}{m} (f_{k-1}^q)^T \mu_k + \frac{\Delta t^2}{m} (f_{k-1}^q)^T \delta_k. \quad (6)$$

Proof. For simplicity we will rewrite the Symplectic Euler by substitution of v_k in (1)

$$\begin{aligned} v_k &= v_{k-1} + \frac{\Delta t}{m} f(v_{k-1}, x_{k-1}, q) \\ x_k &= x_{k-1} + \Delta t \left(v_{k-1} + \frac{\Delta t}{m} f(v_{k-1}, x_{k-1}, q) \right). \end{aligned} \quad (7)$$

The idea is related to [16] for adjoint calculations of iteration equations. We first sum up the products of iterates and unknown multipliers together with the objective (2)

$$\begin{aligned} 0 &= \sum_{k=1}^n \left[v_k - v_{k-1} - \frac{\Delta t}{m} f(v_{k-1}, x_{k-1}, q) \right]^T \mu_k + \\ &\quad \sum_{k=1}^n \left[x_k - x_{k-1} + \Delta t \left(v_{k-1} - \frac{\Delta t}{m} f(v_{k-1}, x_{k-1}, q) \right) \right]^T \delta_k + \\ &\quad J - \sum_{k=1}^n J_k(v_k, x_k, q). \end{aligned} \quad (8)$$

Differentiating w.r.t. control q leads to

$$0 = \sum_{k=1}^n \left[v_k^q - v_{k-1}^q - \frac{\Delta t}{m} f^{v_{k-1}} v_{k-1}^q - \frac{\Delta t}{m} f^{x_{k-1}} x_{k-1}^q - \frac{\Delta t}{m} f_{k-1}^q \right]^T \mu_k + \sum_{k=1}^n \left[x_k^q - x_{k-1}^q + \Delta t \left(v_{k-1}^q - \frac{\Delta t}{m} f^{v_{k-1}} v_{k-1}^q - \frac{\Delta t}{m} f^{x_{k-1}} x_{k-1}^q - \frac{\Delta t}{m} f_{k-1}^q \right) \right]^T \delta_k + J^q - \sum_{k=1}^n (J_k^{v_k})^T v_k^q + (J_k^{x_k})^T x_k^q + J_k^q. \quad (9)$$

Using $x_0^q = v_0^q = 0$, shifting indices in sum and reorder terms for the unknowns x_k^q, v_k^q for $k \in \{1, \dots, n\}$

$$0 = \sum_{k=1}^{n-1} \left[\mu_k - \mu_{k+1} - \frac{\Delta t}{m} (f^{v_k})^T \mu_{k+1} - \frac{\Delta t}{m} \delta_{k+1} - \frac{\Delta t^2}{m} (f^{v_k})^T \delta_{k+1} - J_k^{v_k} \right]^T v_k^q + \sum_{k=1}^{n-1} \left[-\frac{\Delta t}{m} (f^{x_k})^T \mu_{k+1} + \delta_k - \delta_{k+1} - \frac{\Delta t^2}{m} (f^{x_k})^T \delta_{k+1} - J_k^{x_k} \right]^T x_k^q + [\mu_n - J_n^{v_n}]^T v_n^q + [\delta_n - J_n^{x_n}]^T x_n^q + J^q - \sum_{k=1}^n J_k^q - \frac{\Delta t}{m} (f_{k-1}^q)^T \mu_k - \frac{\Delta t^2}{m} (f_{k-1}^q)^T \delta_k. \quad (10)$$

The recursion is finally obtained from the coefficients before the unknown partial derivatives, the final conditions follows from the third line. The sensitivity of the objective function with regards to the control q follows from the last line. \square

Remark. In this paper we will be concerned with a total of N particles in 2-dimensions such that $x_k, v_k \in \mathbb{R}^{2N}$. The recursion (4) can be written as

$$\begin{aligned} \mu_k &= \left(\mathbf{I} + \frac{\Delta t}{m} f^{v_k} \right)^T (\mu_{k+1} + \Delta t \delta_{k+1}) + (J_k^{v_k})^T \\ \delta_k &= \delta_{k+1} + \left(\frac{\Delta t}{m} f^{x_k} \right)^T (\mu_{k+1} + \Delta t \delta_{k+1}) + (J_k^{x_k})^T. \end{aligned} \quad (11)$$

In this form obtained adjoints equal the ones that have been derived earlier by other means [17][18][14].

Remark. We see that in order to control a particle system, we only require the ability to calculate the matrix with partial derivatives of the forces. Further sensitivity calculations need to specify the particle system such as control q . We will restrict to the aforementioned SPH fluids in the following section, where the shape of an obstacle is optimized. The sensitivity is obtained in Section 4.3 by evaluating shape derivative $DJ(\Omega)[\vec{V}_l]$ for domain Ω in direction V_l via formula (6).

3 Smoothed-Particle-Hydrodynamics

Before being concerned with optimization of the SPH flows, Section 3.1 will discuss the basic idea, definitions and notations for this technique, while Section 3.2 is dealing with boundary interactions of SPH particles, that are crucial in shape sensitivity calculations.

3.1 Basics of SPH

Central for SPH-particles travelling on a domain $\Omega \subset \mathbb{R}^d$ is the approximation of the delta distribution by the usage of kernels. Hence, a field value $A : \Omega \rightarrow \mathbb{R}$ is rewritten using the Dirac-Delta identity and approximated in the following sense [6]

$$A(x) = \int A(x') \delta(x - x') dx' \approx \int A(x') W(x - x', h) dx' \approx \sum_{i=1}^N m^i \frac{A^i}{\rho^i} W(x - x^i, h) = A^i \quad (12)$$

for constant particle density ρ^i and particle mass m^i for $i \in \{0, \dots, N\}$, where $W : \mathbb{R}^d \times \mathbb{R}^+ \rightarrow \mathbb{R}$ is defined as a valid kernel if fulfilling properties of normalization, Dirac-Delta limiting such as often positivity, symmetry and compactness of the support [6]. In the literature various valid kernel functions are defined, we restrict ourself here to the original one, hence define the Gaussian kernel as [19]

$$W(x - x^i, h) = \sigma_g \exp \left[-\frac{\|x - x^i\|^2}{h^2} \right] \quad (13)$$

e.g. with two-dimensional normalization as

$$\sigma_g = \frac{1}{\pi h^2}. \quad (14)$$

Remark. The Gaussian kernel comes with the advantage of belonging to class C^∞ , we will use this fact in Section 4. However, it lacks compact support, which results in a summation over all particles in the domain. To counter this, often cut-off kernels as the Cubic Spline [6] or Poly6 [20] kernel are used. In classical form these kernels are not differentiable at the cut-off, but are attractive from computational side, as the summation is only performed over particles in the limited support radius.

Remark. A limited number of publications have been dealing with the convergence of SPH methods, mainly based on joint particle limits $N \rightarrow \infty$ and smoothing limit $h \rightarrow 0$. First attempts relied on spatial discretizations with time-continuous approximations [21] or at least the knowledge about exact particle trajectories [22]. In addition, convergence results have been presented for consecutive limits of discretization parameter and smoothing radius [23] or a selective choice of kernel functions [24].

3.2 Particle Boundary Interactions

Since we are ultimately interested in shape optimization of particle systems, we need to specify the particle boundary interaction. In classical SPH methods, this is typically done via Boundary Particles [6]. The obvious drawback are increased computational efforts, undesired boundary frictions such as the inability to model complex geometries. All SPH boundary techniques have the common idea to approximate the second integral below, which arises naturally when being restricted to a finite domain $\Omega \subset B \subset \mathbb{R}^d$

$$\rho(x) \approx \int_{\Omega} W(x - x', h) \rho(x') dx' + \int_{B \setminus \Omega} W(x - x', h) \rho(x') dx'. \quad (15)$$

In the last decade various researchers addressed this problem e.g. by the usage of continuous boundary methods such as the boundary surface integral method [25] or the signed distance field method [12]. This work will restrict to latter ideas, adjusting whenever appearing necessary in the light of shape optimization. In [12] the boundary density portion ρ_B is set to

$$\rho_B(x) \approx \int_{B \setminus \Omega} \gamma(\eta_{\Omega}(x')) W(x - x', h) dx', \quad (16)$$

where a modification of the signed distance function is used

$$\eta_{\Omega}(x) = s(x) \inf_{x' \in \partial \Omega} \|x - x'\| \text{ with } s(x) = \begin{cases} -1 & \text{if } x \in B \setminus \Omega \\ +1 & \text{otherwise} \end{cases} \quad (17)$$

with

$$\gamma(\eta_{\Omega}) = \begin{cases} \rho_0(1 - \frac{\eta_{\Omega}}{h}) & \text{if } \eta_{\Omega} \leq h \\ 0 & \text{otherwise} \end{cases} \quad (18)$$

for reference density ρ_0 . The implementation in the discretized setting is done via interpolation for each particle and its position x_k^i for $i \in \{0, \dots, N\}$ in each time step by $k \in \{0, \dots, n\}$ on a finite element mesh Ω_h consisting of Lagrangian elements κ , with $S = \frac{(d+p)!}{d!p!}$ nodal degrees of freedom for d dimensions and polynomial order $p \in \mathbb{N}$ with associated shape functions N_s^p , i.e.

$$\rho_{B_h}(x_k^i) = \sum_{s=1}^S m^i \gamma_s N_s^p(x_k^i). \quad (19)$$

The interpolation technique is also used to compute the boundary pressure forces for each article by

$$\mathbf{f}_{B,i,k}^{Pressure} = m^i \nabla_{x_k^i} \rho_{B_h}(x_k^i) \quad (20)$$

for density gradient

$$\nabla \rho_{B_h} = \sum_{s=1}^S \gamma_s \nabla N_s^p. \quad (21)$$

Remark. The advantage in using this boundary representation lies in the possibility to precompute a solution field, allowing cheap finite element interpolations, whenever a particle is in the proximity of the boundary.

Remark. The SDF boundary contribution, introduced in [12], relies on the max-function, i.e.

$$\gamma(\eta_\Omega) = \rho_0 \left(\max(0, 1 - \frac{\eta_\Omega}{h}) \right),$$

since this is not differentiable at $\eta_\Omega = h$, we will use a smoothed max-function in the following section as [26]

$$\max_\alpha(\eta_\Omega) = \begin{cases} \max(0, 1 - \frac{\eta_\Omega}{h}) & \text{for } 1 - \frac{\eta_\Omega}{h} \in \mathbb{R} \setminus [-\frac{1}{\alpha}, \frac{1}{\alpha}] \\ \frac{\alpha}{4}(1 - \frac{\eta_\Omega}{h})^2 - \frac{1}{2}(1 - \frac{\eta_\Omega}{h}) - \frac{1}{4\alpha} & \text{otherwise} \end{cases} \quad (22)$$

for $\alpha > 0$ with derivative as

$$\max'_\alpha(\eta_\Omega) = \begin{cases} 0 & \text{for } 1 - \frac{\eta_\Omega}{h} \in (-\infty, -\frac{1}{\alpha}) \\ -\frac{\alpha}{2h}(1 - \frac{\eta_\Omega}{h}) - \frac{1}{2h} & \text{for } 1 - \frac{\eta_\Omega}{h} \in [-\frac{1}{\alpha}, \frac{1}{\alpha}] \\ -\frac{1}{h} & \text{for } 1 - \frac{\eta_\Omega}{h} \in (\frac{1}{\alpha}, \infty). \end{cases} \quad (23)$$

4 Adjoint-Based Shape Optimization for SPH Particles

The following section is devoted to the derivation of the shape derivative of an SPH-fluid with suitable boundary interaction for a model described in Section 4.1. For this, necessary definitions and notations are recalled in Section 4.2 and applied in Section 4.3. A numerical verification of results for two test cases follows in Section 4.4.

4.1 Model Formulation

Suppose we are given an open domain $\Omega \subset \mathbb{R}^2$, which is split into disjoint subdomains, consisting of a connected, interior domain Ω_1 such that $\Gamma_1 \cup \Gamma_2 \cup \Gamma_3 = \Gamma := \partial\Omega_1$, a simply connected obstacle domain O and an exterior domain $\Omega_2 := \Omega \setminus \bar{\Omega}_1 \setminus O$, such that $\bar{\Omega}_1 \cup \Omega_2 \cup O = \Omega$. We assume the variable, interior boundary Γ_3 and the fixed outer $\Gamma_1 \cup \Gamma_2$ of interior domain Ω_1 to be at least Lipschitz. One simple example of such kind is visualized below in Figure 1.

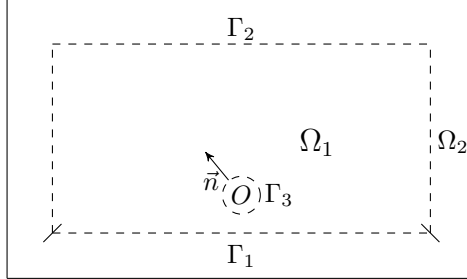


Figure 1: Illustrative Domain $\tilde{\Omega}$ with Initial Circled Obstacle O , Interior Domain Ω_1 , Exterior Domain Ω_2 and Boundaries Γ_1, Γ_2 and Γ_3

On this domain fluids will follow the laws of the incompressible Navier-Stokes equations, i.e. on $\Omega \times (0, T)$ we have

$$\nabla \cdot v = 0 \quad (24)$$

$$-\nabla p + \mu \nabla^2 v + f = \rho \left(\frac{\partial v}{\partial t} + v \cdot \nabla v \right) \quad (25)$$

subject to rigid boundary conditions on $\Omega \times (0, T)$ and suitable initial conditions on $\Omega \times \{0\}$, for scalar density and pressure field $\rho, p : \Omega \rightarrow \mathbb{R}$, vectorial velocity and external force $v, f : \Omega \rightarrow \mathbb{R}^2$ such as viscosity weight $\mu \in \mathbb{R}^+$. Our objective $J : \Omega \rightarrow \mathbb{R}$ consists of three parts

$$J(\Omega) = J_1(\Omega) + J_2(\Omega) + J_3(\Omega). \quad (26)$$

We interpret Γ_1 as coastline and aim for low water heights by setting the first part of objective to

$$J_1(\Omega) = \int_0^T \int_{\Gamma_1} \frac{1}{2} H^2 \, ds \, dt \quad (27)$$

where the water height $H : \Omega \rightarrow \mathbb{R}$ is related to density ρ by the reference density $\rho_0 \in \mathbb{R}^+$ [27]

$$H = \frac{\rho}{\rho_0}. \quad (28)$$

The objective is accompanied by a volume penalty as a second part

$$J_2(\Omega) = \nu_1 \int_O 1 \, dx \quad (29)$$

and a perimeter regularization

$$J_3(\Omega) = \nu_2 \int_{\Gamma_3} 1 \, ds. \quad (30)$$

The contribution of the penalty terms (29) and (30) is controlled by parameters $\nu_1, \nu_2 \in \mathbb{R}^+$, which need to be defined a priori. Finally, with help of (24)-(30) we obtain a PDE-constrained optimization problem, which is intended to be solved via discretize-then-differentiate approach. The discretization is based on SPH as described in Section 3.1 with boundary interaction as in Section 3.2. From this we obtain a particle system with states $X_k = (x_k, v_k) \in \mathbb{R}^{N \times 2} \times \mathbb{R}^{N \times 2}$. Here we interpret Ω_1 as fluid and $\Omega_2 \cup O := B$ as boundary domain for the particles in reference to Section 3.2. Based on this we define the discrete counterpart to objective (27), i.e.

$$\begin{aligned} J_1(\Omega_h) &= \sum_{k=1}^n J_{1,k}(x_k, v_k, \Omega_h) = \sum_{(k,x) \in \{1, \dots, n\} \times \Gamma_{1,h}} \frac{1}{2} \Delta t \left(\frac{\rho(x)}{\rho_0} \right)^2 \\ &= \sum_{(k,x,j) \in \{1, \dots, n\} \times \Gamma_{1,h} \times \{1, \dots, N\}} \frac{1}{2} \Delta t \left(\frac{m}{\rho_0} W(x - x_k^j, h) \right)^2, \end{aligned} \quad (31)$$

where x_k^j defines the position of particle j at time k , that is obtained as solution to an SPH-discretization of the incompressible Navier-Stokes equations.

Remark. By relying on (28) we circumvent the additional carry of information by the individual particles and instead relying on density-based calculation in (31).

Remark. Since particle number and mass are constant over time (24) is naturally fulfilled. In addition, to make the SPH-method applicable for equation (25) the right-hand side is replaced by the material derivative.

Remark. In (31) and in what follows we are relying on a constant particle mass, in line with Section 2. Furthermore in Section 4.2 we omit discretization indices for readability whenever it is clear from the context.

4.2 Basics of Shape Optimization

In this section we introduce methodologies commonly used in shape optimization, extensively elaborated in monographs [28][29][30]. We hereby mainly follow [13]. Starting from a family of mappings $\{\tau_t\}_{t \in [0, \theta]}$ for $\theta > 0$ each current position $x \in \Omega$ is mapped to another by $\tau_t(x)$, where vector field $\vec{V} : \Omega \rightarrow \mathbb{R}^d$ is the direction for the so-called perturbation of identity

$$x_t = \tau_t(x) = x + t\vec{V}(x) \quad (32)$$

Hence, we map the whole domain Ω to another Ω_t such that

$$\Omega_t = \tau_t(\Omega) = \{x_t | x + t\vec{V}(x), x \in \Omega\}. \quad (33)$$

We define the Eulerian Derivative of a generic functional $J : \Omega \rightarrow \mathbb{R}$ as

$$DJ(\Omega)[\vec{V}] = \lim_{t \rightarrow 0^+} \frac{J(\Omega_t) - J(\Omega)}{t}. \quad (34)$$

Commonly, this expression is called shape derivative of J at Ω in direction \vec{V} and in this sense J shape differentiable at Ω if for all directions \vec{V} the Eulerian derivative exists and the mapping $\vec{V} \mapsto DJ(\Omega)[\vec{V}]$ is linear and continuous. In

addition, we define the material derivative of some scalar function $p : \Omega \rightarrow \mathbb{R}$ at $x \in \Omega$ by the derivative of a composed function $p(t) \circ \tau_t : \Omega \rightarrow \Omega_t \rightarrow \mathbb{R}$ as

$$D_m p(x) := \lim_{t \rightarrow 0^+} \frac{p \circ \tau_t(x) - p(x)}{t} = \frac{d}{dt}(p \circ \tau_t)(x) \Big|_{t=0^+} \quad (35)$$

and the corresponding shape derivative for a scalar p as

$$Dp[\vec{V}] := D_m p - \vec{V} \cdot \nabla p. \quad (36)$$

In Section 4.3 we will need the product rule, i.e. [13]

$$D_m(pq) = D_m p q + p D_m q \quad (37)$$

and the fact that material derivatives do not commute with spatial derivatives [13]

$$D_m \nabla p = \nabla D_m p - \nabla \vec{V}^T \nabla p. \quad (38)$$

As mentioned in Section 4.1 we are relying on a discretize-then-differentiate approach. Hence, the perturbation of identity w.r.t. a single vertex perturbation δx_l for vertices $l \in \{1, \dots, L\}$ is defined as [13]

$$\begin{aligned} x_t &= \tau_t(x) \\ &= x + t \delta x_l N_l^1(x) \\ &= x + t \vec{V}_l(x), \end{aligned} \quad (39)$$

where N_l^1 is a finite-element basis function of first order, i.e. a continuous piecewise-linear polynomial.

Remark. The ultimate position $x_t \in \Omega_t$ can be calculated using summed vertex contributions, i.e.

$$x_t = x + t \sum_{l=1}^L \delta x_l N_l^1(x). \quad (40)$$

The discretized perturbation of identity interpolates the deformation $t \delta x_l$ of vertex $l \in \{1, \dots, L\}$ on the support of N_l^1 .

4.3 Adjoint-Based Shape Optimization for SPH Particles

The sensitivity with respect to domain deformations is obtained from Theorem 1 as

$$D J_1(\Omega)[\vec{V}] = \frac{d J_1(\Omega_t)}{dt} \Big|_{t=0^+} = \frac{d}{dt} \sum_{k=1}^n J_{1,k}(x_k, v_k, \Omega_t) \Big|_{t=0^+} + \frac{d}{dt} \sum_{k=1}^n (f_{k-1}^t)^T \left(\frac{\Delta t}{m} \mu_k + \frac{\Delta t^2}{m} \delta_k \right) \Big|_{t=0^+}, \quad (41)$$

where occurring functions are defined on the perturbed domain $\Omega_t \subset \mathbb{R}^d$. In need of deriving the shape derivative, we firstly state the following lemma for Lagrangian finite elements [13]

Lemma 2. *For a finite element function $g \in V_h \subset H^1(\Omega)$, i.e. $g(x) = \sum_{s=1}^S g_s N_s^p(x)$ for finite element ansatz function N_s^p , whose restriction on an Lagrangian element κ is a polynomial of order $p \geq 1$, the shape derivative is derived as*

$$Dg[\vec{V}] = \sum_{s=1}^S (Dg_s[\vec{V}] N_s^p - g_s \vec{V} \cdot \nabla N_s^p), \quad (42)$$

where $N_s^p(x_t) = N_s^p(\tau_t^{-1}(x_t))$ is moving along the deformation.

Proof. [13] Since $N_s^p(x)$ is moving along the deformation, the material derivative vanishes

$$D_m N_s^p = 0$$

hence for the shape derivative it holds by (36)

$$D N_s^p[\vec{V}] = -\vec{V} \cdot \nabla N_s^p.$$

Since g_s is spatially constant, we conclude according to [13]

$$D_m g = \sum_{s=1}^S Dg_s[\vec{V}] N_s^p$$

and therefore obtain the shape derivative as

$$Dg[\vec{V}_l] = D_m g - \vec{V}_l \nabla g = \sum_{s=1}^S \left(Dg_s[\vec{V}_l] N_s^p - g_s \vec{V}_l \cdot \nabla N_s^p \right).$$

□

Remark. For SPH boundary computations we recall the shape derivative of the signed distance [30]

$$D\eta_\Omega(x)[\vec{V}] = -\vec{V}(P_{\partial\Omega}(x)) \cdot \vec{n}(P_{\partial\Omega}(x)) \quad (43)$$

with operator $P_{\partial\Omega}$ that projects a point $x \in \Omega$ onto its closest boundary and holds for all $x \notin \Sigma$, where Σ is referred to as the ridge. In this sense, $D\eta_{\Omega,s}[\vec{V}_l]$ is its nodal discretized counterpart w.r.t. the l^{th} vertex perturbation.

Since the boundary contribution is driven by pressure forces (20), we require the shape derivative of the gradient of a finite element function (21).

Lemma 3. *For the gradient of a finite element function, i.e. $\nabla g(x) = \sum_{s=1}^S g_s \nabla N_s^p(x)$ for finite element ansatz function N_s^p , whose restriction on an Lagrangian element κ is a polynomial of order $p \geq 2$, the shape derivative is derived as*

$$D(\nabla g)[\vec{V}_l] = \sum_{s=1}^S Dg_s[\vec{V}_l] \nabla N_s^p - \left(\nabla \vec{V}_l \right)^T \left(\sum_{s=1}^S g_s \nabla N_s^p \right) - \nabla \left(\sum_{s=1}^S g_s \nabla N_s^p \right) \vec{V}_l. \quad (44)$$

Proof. The material derivative does not commute with the spatial derivative (38)

$$D_m(\nabla g) = \nabla(D_m g) - \left(\nabla \vec{V}_l \right)^T \nabla g \quad (45)$$

which equals by the same argument as in proof to Lemma 2

$$D_m(\nabla g) = \nabla \left(\sum_{s=1}^S Dg_s[\vec{V}_l] N_s^p \right) - \left(\nabla \vec{V}_l \right)^T \left(\sum_{s=1}^S g_s \nabla N_s^p \right). \quad (46)$$

Then we have for the shape derivative

$$\begin{aligned} D(\nabla g)[\vec{V}_l] &= D_m(\nabla g) - \nabla(\nabla g)\vec{V}_l \\ &= \nabla \left(\sum_{s=1}^S Dg_s[\vec{V}_l] N_s^p \right) - \left(\nabla \vec{V}_l \right)^T \left(\sum_{s=1}^S g_s \nabla N_s^p \right) - \nabla \left(\sum_{s=1}^S g_s \nabla N_s^p \right) \vec{V}_l. \end{aligned} \quad (47)$$

□

Theorem 4. *Assume $\{x_k\}_{k=1}^n$ moves alongside the deformation, the shape derivative of objective J_1 is then given by*

$$\begin{aligned} DJ_1(\Omega)[\vec{V}_l] &= \frac{d}{dt} \sum_{k=1}^n J_{1,k}(x_k, v_k, \Omega_t) \Big|_{t=0^+} + \frac{d}{dt} \sum_{k=1}^n (f_{k-1}^t)^T \left(\frac{\Delta t}{m} \mu_k + \frac{\Delta t^2}{m} \delta_k \right) \Big|_{t=0^+} \\ &= \sum_{k=1}^n \sum_{i=1}^N \left[\nabla \left(\sum_{s=1}^S D\gamma_s[\vec{V}_l] N_s^p(\mathbf{x}_k^i) \right) - \left(\nabla \vec{V}_l(\mathbf{x}_k^i) \right)^T \left(\sum_{s=1}^S \gamma_s \nabla N_s^p(\mathbf{x}_k^i) \right) - \right. \\ &\quad \left. \nabla \left(\sum_{s=1}^S \gamma_s \nabla N_s^p(\mathbf{x}_k^i) \right) \vec{V}_l(\mathbf{x}_k^i) \right]^T (\Delta t \mu_k^i + \Delta t^2 \delta_k^i), \end{aligned} \quad (48)$$

where $D\gamma_s[\vec{V}_l]$ is the nodal discretization w.r.t. the l^{th} vertex perturbation of

$$D\gamma(x)[\vec{V}] = \max'_\alpha(\eta_\Omega(x))(-\vec{V}(P_{\partial\Omega}(x)) \cdot \vec{n}(P_{\partial\Omega}(x))). \quad (49)$$

Proof. Since Γ_1 is fixed, the objective (31) is independent of mesh deformations. Hence, the shape derivative is zero, i.e.

$$\frac{d}{dt} \sum_{k=1}^n J_{1,k}(x_k, v_k, \Omega_t) \Big|_{t=0^+} = 0.$$

We recall that for SPH-flows the fluid and boundary part are split up (15), i.e. for density of particle $i \in \{1, \dots, N\}$ in each time step $k \in \{1, \dots, n\}$

$$\rho(x_k^i) = \sum_{j=1}^N mW(x_k^i - x_k^j, h) + \sum_{s=1}^S mN_s(x_k^i) \gamma_s.$$

The first sum is only dependent on the position of the particles, hence the respective shape derivatives vanish due to adjoints and we have

$$\left. \frac{d}{dt} \sum_{j=1}^N mW(x_k^i - x_k^j, h) \right|_{t=0^+} = 0.$$

The remainders follow from regarding pressure terms (21), Lemma 2 and 3 such as equation (48), by assuming that the particle position $\{x_k^i\}_{k=1}^n$ moves alongside the deformation. \square

Remark. The assumption that $\{x_k\}_{k=1}^n$ moves along the deformation drastically simplifies calculations, otherwise we are required to perform low-level computations similar to [14].

Remark. Using (39) and the fact that nodal values are spatially constant we can rewrite (48) as

$$\begin{aligned} DJ_1(\Omega)[\vec{V}_l] &= \frac{d}{dt} \sum_{k=1}^n (f_{k-1}^t)^T \left(\frac{\Delta t}{m} \mu_k + \frac{\Delta t^2}{m} \delta_k \right) \Big|_{t=0^+} \\ &= \sum_{k=1}^n \sum_{i=1}^N \left[\left(\sum_{s=1}^S D\gamma_s[\vec{V}_l] \nabla N_s^p(x_k^i) \right) - \left(\delta x_l \nabla N_l^1(x_k^i) \right)^T \left(\sum_{s=1}^S \gamma_s \nabla N_s^p(x_k^i) \right) - \right. \\ &\quad \left. \left(\sum_{s=1}^S \gamma_s \nabla \nabla N_s^p(x_k^i) \right) \delta x_l N_l^1(x_k^i) \right]^T (\Delta t \mu_k^i + \Delta t^2 \delta_k^i). \end{aligned} \quad (50)$$

Here we highlight, that the product of ansatz functions is zero, whenever, x_k^i is not in the support of shape functions N_s^p and N_l^1 .

Remark. Factoring out the respective δx_l in (50) we can calculate the remaining quantities of size d for each mesh vertex perturbation. All quantities can be collected in a vector DJ_1 of size dL to apply some mesh deformation strategy as discussed in [31]. Linear elasticity calculations as in [32] can be enabled, by choosing a basis of the test function space, calculating all occurring quantities and split vectorial contributions, as it is common in vector-valued Finite Element Methods.

Remark. For completeness shape derivatives of the penalty terms (29) and (30) are obtained as [29]

$$DJ_2(\Omega)[\vec{V}] = \nu_1 \int_{\Omega} \nabla \cdot \vec{V} \, dx \quad (51)$$

$$DJ_3(\Omega)[\vec{V}] = \nu_2 \int_{\Gamma_3} \kappa \langle \vec{V}, \vec{n} \rangle \, ds = \nu_2 \int_{\Gamma_3} \nabla \cdot \vec{V} - \langle \frac{\partial \vec{V}}{\partial \vec{n}}, \vec{n} \rangle \, ds. \quad (52)$$

The discretization of (51) and (52) and the subsequent usage in optimization routines follows naturally for standard finite element solvers [15].

4.4 Numerical Results

In this section we will first give details about the numerical implementation, before verifying results for a selected choice of test cases.

The SPH techniques from Section 3 to solve incompressible Navier-Stokes equations with boundary contributions can be summarized in a pseudocode as

Algorithm 1: 2D SPH for NS with Boundary Contribution

Initialize Particle $i \in \{1, \dots, N\}$ carrying $X_k^i = \langle v_k^i, x_k^i \rangle$ for each Time Step $k \in \{0, \dots, n\}$ with Mass m and step-size Δt ;

foreach Particle i **do**

- | Find Neighbour Particles j

end

foreach Particle i **do**

- | Compute Fluid Density: $\rho_F^i = \sum_j mW(x^i - x^j, h)$
- | Compute Fluid Pressure: $p_F^i = B \left[\left(\frac{\rho^i}{\rho_0} \right)^\xi - 1 \right]$
- | Compute Boundary Density: $\rho_B^i = \sum_s m\gamma_s N_s^p(x^i)$

end

foreach Particle i **do**

- | Calculate Forces:
- | $\mathbf{f}_i^{Pressure} = \mathbf{f}_{F,i}^{Pressure} + \mathbf{f}_{B,i}^{Pressure}$
- | $\mathbf{f}_i^{Viscosity}$
- | $\mathbf{f}_i^a = \mathbf{f}_i^{Pressure} + \mathbf{f}_i^{Viscosity}$

end

foreach Particle i **do**

- | Calculate States:
- | $\mathbf{v}_{k+1}^i = \mathbf{v}_k^i + \Delta t \mathbf{f}_k^i / m$
- | $\mathbf{x}_{k+1}^i = \mathbf{x}_k^i + \Delta t \mathbf{v}_{k+1}^i$

end

Remark. The neighbour search is only mentioned for completeness. For the Gaussian kernel (13), the search for neighbouring particles is trivially omitted.

Remark. For simplicity external forces are zeroed in (25). Additional forces, as e.g. gravitational or repulsive forces would require a specific adjoint treatment [18]. Fluid pressure and viscosity forces are calculated density-dependent as

$$\mathbf{f}_{F,i}^{Pressure} = - \sum_j m \frac{p_F^i + p_F^j}{2\rho_F^j} \nabla_i W(x^i - x^j, h) \quad (53)$$

$$\mathbf{f}_i^{Viscosity} = \mu \sum_j \frac{v^j - v^i}{\rho^j} \nabla_i^2 W(x^i - x^j, h). \quad (54)$$

In addition, we have used Tait's law to compute the water pressure with $B = 0.3214$ and $\xi = 7$ [33].

In all the following examples we will work with a simple mesh in line with definitions given in Section 4.3, as it can be seen in Figure 2. The precomputed solution for the initial mesh can be taken from Figure 3. The solution to the signed

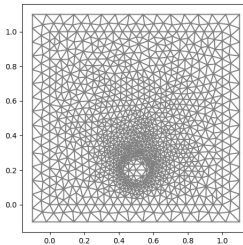


Figure 2: Initial Particle Mesh Ω_h

distance function is based on the solution of the Eikonal Equation with $f(x) = 1$, $q(x) = 0$

$$\begin{aligned} |\nabla w(x)| &= f(x) & x \in \Omega \\ w(x) &= q(x) & x \in \Gamma, \end{aligned} \quad (55)$$

where we have implemented a viscous and stabilized version to obtain $w \in H^1(\Omega)$ for all $v \in H^1(\Omega)$ i.e.

$$\int_{\Omega} \sqrt{\nabla w \nabla w} \, dx - \int_{\Omega} f v \, dx + \int_{\Omega} \epsilon_{SDF} \nabla w \nabla v \, dx = 0, \quad (56)$$

where $\epsilon_{SDF} = \max h_{\kappa}$ is dependent on the element-diameter h_{κ} of cell $\kappa \in \Omega_h$. Build on this solution, modifications as in (22) are exercised downstream by prescribing respective nodal values.

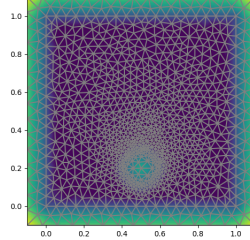


Figure 3: Precomputed Modification of Signed Distance Function for Initial Mesh Ω_h

The recursive adjoints require the calculation of a matrix with partial derivatives w.r.t. the states. The partial derivatives matrix w.r.t. the positions is obtained by a $2n \times 2n$ matrix

$$\frac{\partial f}{\partial x} = \begin{pmatrix} \frac{\partial f_1^x}{\partial x^1} & \frac{\partial f_1^x}{\partial x^2} & \cdots & \frac{\partial f_1^x}{\partial x^n} & \frac{\partial f_1^x}{\partial y^1} & \frac{\partial f_1^x}{\partial y^2} & \cdots & \frac{\partial f_1^x}{\partial y^n} \\ \frac{\partial f_2^x}{\partial x^1} & \ddots & & \vdots & \frac{\partial f_2^x}{\partial y^1} & \ddots & & \vdots \\ \vdots & & \ddots & & \vdots & & \ddots & \vdots \\ \frac{\partial f_n^x}{\partial x^1} & \cdots & \cdots & \frac{\partial f_n^x}{\partial x^n} & \frac{\partial f_n^x}{\partial y^1} & \cdots & \cdots & \frac{\partial f_n^x}{\partial y^n} \\ \frac{\partial f_1^y}{\partial x^1} & \frac{\partial f_1^y}{\partial x^2} & \cdots & \frac{\partial f_1^y}{\partial x^n} & \frac{\partial f_1^y}{\partial y^1} & \frac{\partial f_1^y}{\partial y^2} & \cdots & \frac{\partial f_1^y}{\partial y^n} \\ \frac{\partial f_2^y}{\partial x^1} & \ddots & & \vdots & \frac{\partial f_2^y}{\partial y^1} & \ddots & & \vdots \\ \vdots & & \ddots & & \vdots & & \ddots & \vdots \\ \frac{\partial f_n^y}{\partial x^1} & \cdots & \cdots & \frac{\partial f_n^y}{\partial x^n} & \frac{\partial f_n^y}{\partial y^1} & \cdots & \cdots & \frac{\partial f_n^y}{\partial y^n} \end{pmatrix} \quad (57)$$

and the $2n \times 2n$ matrix of partial derivatives of the particle velocities as

$$\frac{\partial f}{\partial v} = \begin{pmatrix} \frac{\partial f_1^x}{\partial u^1} & \frac{\partial f_1^x}{\partial u^2} & \cdots & \frac{\partial f_1^x}{\partial u^n} & \frac{\partial f_1^x}{\partial v^1} & \frac{\partial f_1^x}{\partial v^2} & \cdots & \frac{\partial f_1^x}{\partial v^n} \\ \frac{\partial f_2^x}{\partial u^1} & \ddots & & \vdots & \frac{\partial f_2^x}{\partial v^1} & \ddots & & \vdots \\ \vdots & & \ddots & & \vdots & & \ddots & \vdots \\ \frac{\partial f_n^x}{\partial u^1} & \cdots & \cdots & \frac{\partial f_n^x}{\partial u^n} & \frac{\partial f_n^x}{\partial v^1} & \cdots & \cdots & \frac{\partial f_n^x}{\partial v^n} \\ \frac{\partial f_1^y}{\partial u^1} & \frac{\partial f_1^y}{\partial u^2} & \cdots & \frac{\partial f_1^y}{\partial u^n} & \frac{\partial f_1^y}{\partial v^1} & \frac{\partial f_1^y}{\partial v^2} & \cdots & \frac{\partial f_1^y}{\partial v^n} \\ \frac{\partial f_2^y}{\partial u^1} & \ddots & & \vdots & \frac{\partial f_2^y}{\partial v^1} & \ddots & & \vdots \\ \vdots & & \ddots & & \vdots & & \ddots & \vdots \\ \frac{\partial f_n^y}{\partial u^1} & \cdots & \cdots & \frac{\partial f_n^y}{\partial u^n} & \frac{\partial f_n^y}{\partial v^1} & \cdots & \cdots & \frac{\partial f_n^y}{\partial v^n} \end{pmatrix} \quad (58)$$

In the continuous setting, a deformation scheme can be obtained by regarding the Steklov-Poincaré metric [15], such that a solution of the linear elasticity equation $\vec{W} : \Omega \rightarrow \mathbb{R}^2$ can be used, i.e.

$$\begin{aligned} \int \sigma(\vec{W}) : \epsilon(\vec{V}) = DJ[\vec{V}] & \quad \forall \vec{V} \in H_0^1(\Omega, \mathbb{R}^2) \\ \sigma &:= \lambda \text{Tr}(\epsilon(\vec{W})) \mathbf{I} + 2\mu \epsilon(\vec{W}) \\ \epsilon(\vec{W}) &:= \frac{1}{2}(\nabla \vec{W} + \nabla \vec{W}^T) \\ \epsilon(\vec{V}) &:= \frac{1}{2}(\nabla \vec{V} + \nabla \vec{V}^T), \end{aligned} \quad (59)$$

where σ and ϵ are called strain and stress tensor and λ and μ are called Lamé parameters. We have chosen $\lambda = 0$ and μ as the solution of the following Poisson Problem

$$\begin{aligned} -\Delta \mu &= 0 && \text{in } \Omega \\ \mu &= \mu_{max} && \text{on } \Gamma_3 \\ \mu &= \mu_{min} && \text{on } \Gamma_1, \Gamma_2. \end{aligned} \tag{60}$$

In our discrete setting, the right hand-side in (59) is manually evaluated using (50) and the associated remark. The full gradient-descent based shape optimization algorithm for SPH-flows is pseudocoded below.

Algorithm 2: SPH Shape Optimization Algorithm

Initialization Mesh, Particles

```

while  $||D\mathcal{J}(\Omega_t)[\vec{V}]|| > \epsilon$  do
    1 Calculate Modified SDF  $\gamma_t$  [via Viscous Eikonal Eq. (56)]
    2 Calculate States  $x_t, v_t$  [via SPH Algorithm 1]
    3 Calculate Adjoints  $\delta_t, \mu_t$  [via Section 2 & AD]
    4 Calculate Gradient  $W_t$  [via Eq. (50-52) & Linear Elasticity (59)]
    5 Perform Linesearch for  $\tilde{W}_t$ 
    6 Calculate  $\Omega_{t+1}$  [via  $\tilde{W}_t$  and Eq. (39)]
end

```

Remark. Calculation of partial derivatives in (57) and (58), associated with Step 3, is analytically possible, however results in a tremendous calculative effort, prone to errors. For circumvention we use automatic differentiation (AD) via the Autograd¹ library in either a forward or backward mode for the fluid portion, which is possible for code generated fully in Numpy². Here we highlight for boundary terms as defined in (19) the partial derivative matrix for positional state is diagonal and zero for the velocity state. The derivatives of the boundary contributions are fully implemented in FEniCS [34]. The manual evaluation of (50) in Step 4 is relying on a constant evaluation of finite element ansatz functions, where the FEniCS build-in function *evaluate_basis_derivatives_all* is used.

Example 1:

In the first example we model the propagation of two particles, i.e. $N = 2$, with initial position $x_0^1 = (0.5, 0.5)$ and $x_0^2 = (0.63, 0.5)$, towards the shore by prescribing initial velocities as $v_0 = (0, -3)^2$. This test case is deliberately kept simple to analyse the procedure. In Figure 4 we have visualized the particle movements for time snapshots $t \in \{0, 0.6, 0.12, 0.18\}$ for smoothing radius $h = 0.04$, particle mass $m = 1$, smoothing factor $\alpha = 100$ and reference density $\rho_0 = 10$. The particle propagation is performed using time steps of size $\Delta t = 0.008$ with end time $T = 0.18$. The red particle, with initial position x_0^1 , travels towards the shore Γ_1 and effectively accounts for an increased objective in form of (31), while the blue, with initial position x_0^2 , is reflected from the obstacle and travels back into the field only marginally contributing to the objective. Both particles are within the interaction radius of the obstacle for a certain time frame, such that shape derivatives of pressure forces are non-zero. However, as stated above, the objective contribution of blue ensures that adjoints $\{\delta_k\}_{k=1}^n$ and $\{\mu_k\}_{k=1}^n$ are vanishingly small. The deformation vector is hence predominantly activated in reds interaction region with the obstacle, as it can be observed in Figure 5 on the left. Relying on the shape optimization algorithm that we have presented before, for initial step-size $\tau = 0.0001$ and tolerance $\epsilon = 1E - 9$, we are able to deform the obstacle setting $\mu_{min} = 10$ and $\mu_{max} = 100$. The final mesh is able to decrease the objective up to a minimum, as it can be seen in Figure 5 in the mid and right part. We highlight, that even a small deformation is able to achieve these results in this simple setting.

¹<https://github.com/HIPS/autograd>

²<https://numpy.org/>

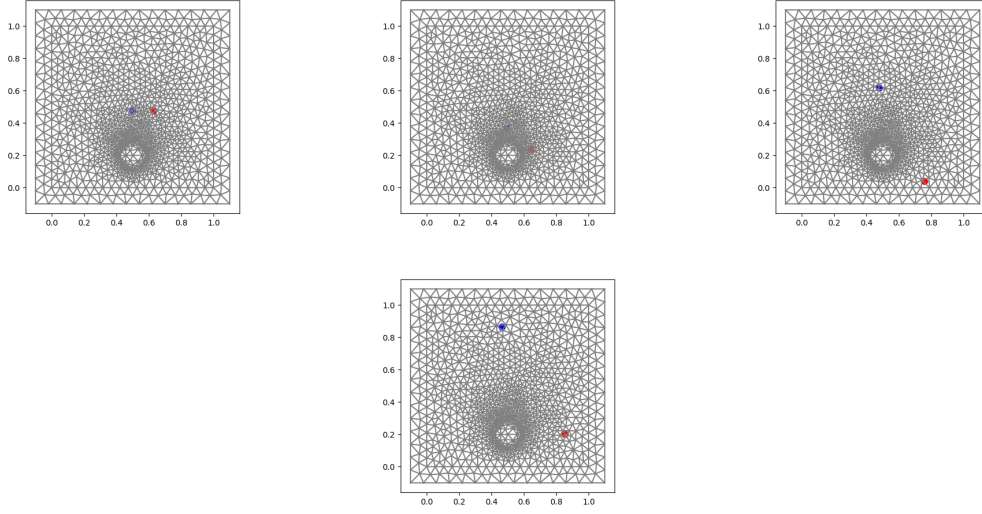


Figure 4: Ex.1 Particle Propagation for $t \in \{0, 0.6, 0.12, 0.18\}$

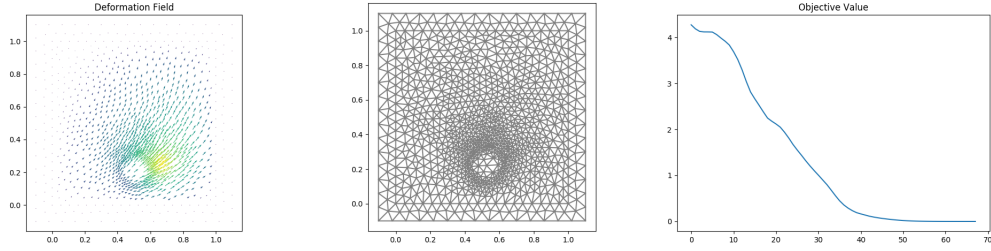


Figure 5: Ex.1 Deformation Field, Final Mesh, Objective

Example 2:

In the second example we increase the number of particles, i.e. $N = 180$, with initial positions drawn from a normal distribution as $x_0 = (0.55 + \mathcal{N}(0, 0.1), 0.6 + \mathcal{N}(0, 0.1))^N$. The particles once more travel towards the shore driven by initial velocity as $v_0 = (0, -1)^N$. The remaining settings are as in the first example. We can observe the movement in Figure 6.

Once more relying on our shape optimization algorithm, we are able to deform the obstacle using the resulting deformation field, pictured in Figure 7 on the left. In this setting a larger deformation is necessary to effectively reduce the objective as we see in the final mesh Figure 7 in the middle and on the right. We would like to highlight that the performance of the algorithm can be degrading by particle and boundary interactions, resulting from mesh movements. Potentially this hinders us from obtaining improved results.

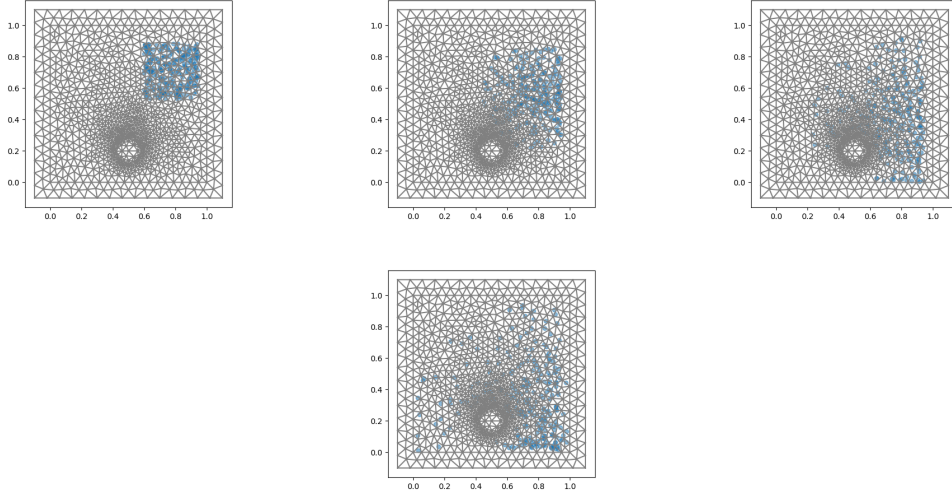
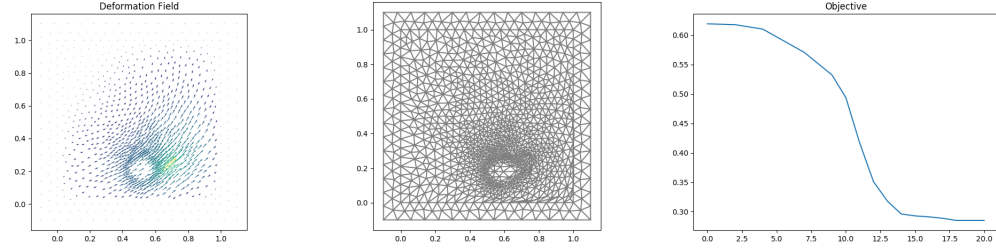
Figure 6: Ex.2 Particle Propagation for $t \in \{0, 0.6, 0.12, 0.18\}$ 

Figure 7: Ex.2 Deformation Field, Final Mesh, Objective

5 Conclusion

We have derived the discrete adjoint for a general Symplectic Euler particle class, in addition for an SPH-representative, based on boundary interactions by signed distance fields, the shape derivative was derived, that reduces to the shape derivative of a finite element interpolator. Results have been verified on a sample mesh inspired by practical applications to mitigate effects of coastal erosion. We point out that this can only serve as a first feasibility study, since the number of particles is still low and meshes are simplified. In future, comparisons between shape optimization results in an Eulerian, cf. to [35] and [36], and an Lagrangian framework with extensions to shallow water equations, as in [27], such as an Eulerian-Lagrangian coupling e.g. for a Shallow-Water-Exner model, appear of interest.

Acknowledgement

This work has been supported by the Deutsche Forschungsgemeinschaft within the Priority program SPP 1962 "Non-smooth and Complementarity-based Distributed Parameter Systems: Simulation and Hierarchical Optimization". The authors would like to thank Diaraf Seck (Université Cheikh Anta Diop, Dakar, Senegal) and Mame Gor Ngom (Université Cheikh Anta Diop, Dakar, Senegal) for helpful and interesting discussions within the project Shape Optimization Mitigating Coastal Erosion (SOMICE).

References

- [1] Bernard Nayroles, Gilbert Touzot, and Pierre Villon. Generalizing the finite element method: Diffuse approximation and diffuse elements. *Computational Mechanics*, 10:307–318, 1992.
- [2] T. Belytschko, Y. Y. Lu, and L. Gu. Element-free galerkin methods. *International Journal for Numerical Methods in Engineering*, 37(2):229–256, 1994.

- [3] Wing Kam Liu, Sukky Jun, and Yi Fei Zhang. Reproducing kernel particle methods. *International Journal for Numerical Methods in Fluids*, 20(8-9):1081–1106, 1995.
- [4] Seiichi Koshizuka and Yoshiaki Oka. Moving-particle semi-implicit method for fragmentation of incompressible fluid. *Nuclear Science and Engineering*, 123:421–434, 1996.
- [5] Yoshifumi Ogami and Teruaki Akamatsu. Viscous flow simulation using the discrete vortex model—the diffusion velocity method. *Computers & Fluids*, 19(3):433–441, 1991.
- [6] Joseph Monaghan. Sph compressible turbulence. *Monthly Notices of the Royal Astronomical Society*, 335, 04 2002.
- [7] Florin Bobaru. Meshless approach to shape optimization of linear thermoelastic solids. *International Journal for Numerical Methods in Engineering*, 53:765 – 796, 02 2002.
- [8] Iulian Grinoreanu, Kuang-Hua Chang, Jiun-Shyan Chen, and Kyung Choi. Design sensitivity analysis of hyperelastic structures using a meshless method. *Aiaa Journal - AIAA J*, 36:618–627, 04 1998.
- [9] J. Chen and Nam Kim. *Meshfree Method and Application to Shape Optimization*, pages 389–414. World Scientific, 09 2007.
- [10] Raphael Hohmann and Christian Leithäuser. Gradient-based shape optimization for the reduction of particle erosion in bended pipes, 2019.
- [11] Youn Doh Ha, Min-GEUN Kim, Hyun-seok Kim, and Seonho Cho. Shape design optimization of sph fluid–structure interactions considering geometrically exact interfaces. *Structural and Multidisciplinary Optimization*, 44:319–336, 09 2011.
- [12] Dan Koschier and Jan Bender. Density maps for improved sph boundary handling. *Proceedings of the ACM SIGGRAPH / Eurographics Symposium on Computer Animation*, 2017.
- [13] Martin Berggren. A unified discrete-continuous sensitivity analysis method for shape optimization. In *CSC 2010*, 2010.
- [14] René Schneider and Peter Jimack. On the evaluation of finite element sensitivities to nodal coordinates. *Electronic Transactions on Numerical Analysis. Volume*, 32:134–144, 01 2008.
- [15] Volker H. Schulz, Martin. Siebenborn, and Kathrin. Welker. Efficient pde constrained shape optimization based on steklov–poincaré-type metrics. *SIAM Journal on Optimization*, 26(4):2800–2819, 2016.
- [16] V. H. Schulz. Numerical optimization of the cross-sectional shape of turbine blades, 1996.
- [17] Antoine McNamara, Adrien Treuille, Zoran Popović, and Jos Stam. Fluid control using the adjoint method. *ACM Trans. Graph.*, 23(3):449–456, August 2004.
- [18] C. Wojtan, P. Mucha, and Greg Turk. Keyframe control of complex particle systems using the adjoint method. In *SCA '06*, 2006.
- [19] Joseph John Monaghan and John Lattanzio. A refined particle method for astrophysical problems. *Astronomy and Astrophysics*, 149:135–143, 1985.
- [20] Matthias Müller, David Charypar, and Markus H. Gross. Particle-based fluid simulation for interactive applications. In *SCA '03*, 2003.
- [21] P. A. Raviart. An analysis of particle methods. In Franco Brezzi, editor, *Numerical Methods in Fluid Dynamics*, pages 243–324, Berlin, Heidelberg, 1985. Springer Berlin Heidelberg.
- [22] B. Ben Moussa and J. P. Vila. Convergence of sph method for scalar nonlinear conservation laws. *SIAM Journal on Numerical Analysis*, 37(3):863–887, 2000.
- [23] R. Di Lisio, E. Grenier, and M. Pulvirenti. The convergence of the sph method. *Computers & Mathematics with Applications*, 35(1):95–102, 1998.
- [24] K. Oelschläger. *On the Connection Between Hamiltonian Many-particle Systems and the Hydrodynamical Equations*. Universität Heidelberg. SFB 123, 1991.
- [25] Sivakumar Kulasegaram, Javier Bonet, Roland Lewis, and Matthew Profit. A variational formulation based contact algorithm for rigid boundaries in 2d sph applications. *Computational Mechanics*, 33:316–325, 03 2004.
- [26] Constantin Christof, Christian Clason, Christian Meyer, and Stephan Walther. Optimal control of a non-smooth semilinear elliptic equation. *Mathematical Control and Related Fields (MCRF)*, 8:247–276, 05 2017.
- [27] Barbara Solenthaler, Peter Bucher, Nuttapon Chentanez, Matthias Müller, and Markus Gross. SPH Based Shallow Water Simulation. In Jan Bender, Kenny Erleben, and Eric Galin, editors, *Workshop in Virtual Reality Interactions and Physical Simulation "VRIPHYS"* (2011). The Eurographics Association, 2011.

- [28] Kyung K. Choi. Shape design sensitivity analysis and optimal design of structural systems. In Carlos A. Mota Soares, editor, *Computer Aided Optimal Design: Structural and Mechanical Systems*, pages 439–492, Berlin, Heidelberg, 1987. Springer Berlin Heidelberg.
- [29] J. Sokołowski and J.P. Zolésio. *Introduction to shape optimization: shape sensitivity analysis*. Springer series in computational mathematics. Springer-Verlag, 1992.
- [30] M. C. Delfour and J. P. Zolésio. *Shapes and Geometries*. Society for Industrial and Applied Mathematics, second edition, 2011.
- [31] Bijan Mohammadi and Olivier Pironneau. Applied shape optimization in fluids. *Applied Shape Optimization for Fluids*, 05 2001.
- [32] Timothy J. Baker and Peter A. Cavallo. Dynamic adaptation for deforming tetrahedral meshes. In *14th Computational Fluid Dynamics Conference*, 1999.
- [33] Markus Becker and Matthias Teschner. Weakly compressible sph for free surface flows. In Dimitris Metaxas and Jovan Popovic, editors, *Eurographics/SIGGRAPH Symposium on Computer Animation*. The Eurographics Association, 2007.
- [34] Martin S. Alnæs, Jan Blechta, Johan Hake, August Johansson, Benjamin Kehlet, Anders Logg, Chris Richardson, Johannes Ring, Marie E. Rognes, and Garth N. Wells. The fenics project version 1.5. *Archive of Numerical Software*, 3(100), 2015.
- [35] Luka Schlegel and Volker Schulz. Shape optimization for the mitigation of coastal erosion via shallow water equations, 2021.
- [36] Luka Schlegel and Volker Schulz. Shape optimization for the mitigation of coastal erosion via porous shallow water equations, 2021.